Octupole correlation effects on two-neutron transfer intensity in rare-earth nuclei

Kosuke Nomura*
Department of Physics, Hokkaido University, Sapporo 060-0810, Japan and
Nuclear Reaction Data Center, Hokkaido University, Sapporo 060-0810, Japan
(Dated: April 18, 2026)

Impacts of octupole correlations on the low-lying 0^+ states and two-neutron transfer intensities in rare-earth nuclei are investigated in terms of the interacting boson model that is based on the nuclear density functional theory. The octupole degrees of freedom are not only essential building blocks to describe properties of negative-parity states in the model, but also influence low-spin positive-parity states including excited 0^+ states. The calculation produces a large number of low-energy 0^+ states that contain significant amounts of octupole components, indicating important roles played by the octupole degrees freedom in this mass region. Octupole correlations are shown to make sizable contributions to the (p,t) and (t,p) transfer intensities and, in particular, to reproduce the discontinuous changes of these quantities near those nuclei with $N \approx 88$ or 90, which are observed experimentally as a signature of the shape phase transition.

I. INTRODUCTION

Reflection asymmetric, octupole shapes in atomic nuclei have attracted considerable interest in the field of nuclear physics [1–5]. Up to the present, evidence for a static octupole shape was suggested experimentally in a few nuclides in light actinide (e.g., ^{220}Rn [6], ^{224}Ra [6]), rare-earth and lanthanide (e.g, ^{144}Ba [7], and ^{146}Ba [8]) regions. These nuclei exhibit a low-energy negative-parity band, which forms an alternating-parity band with the positive-parity ground-state band, connected by strong electric dipole ($E1$) and octupole ($E3$) transitions. The octupole correlations are expected to be enhanced for those nuclei with neutron N and/or proton Z numbers approximately equal to 34, 56, 88, 134, ..., for which the coupling of single-particle states that differ by $\Delta j = \Delta l = 3$ is possible. While there are only a few instances that are empirically suggested to exhibit the static octupole deformation, the octupole shape degrees of freedom are still expected to be a relevant ingredient to determine various low-energy nuclear structure phenomena.

In the light actinide and rare-earth regions, in addition to the low-energy negative-parity bands that are of octupole character, low-lying excited 0^+ states and the bands built on them have been observed. The low-energy 0^+ states are often attributed to the intruder states that are different in intrinsic structure from the ground state [9–13]. In addition, the observed second 0^+ energy levels in rare-earth nuclei are known to become particularly low in the vicinity of $N \approx 90$, and this systematic is recognized as a signature of the quantum phase transition (QPT) [14–17] in nuclear shapes from nearly spherical to strongly prolate deformed configurations. Another interpretation of the low-lying 0^+ levels has been made in terms of the pairing degrees of freedom [18–26]. The presence of the 0^+ bands has also been considered to be a consequence of the coupling of two octupole phonons (see Ref. [3] and references therein).

Here the two-neutron transfer, i.e., (p,t) and (t,p), reactions are of special interest. These nuclear reactions have been frequently used in experiments to investigate pairing properties and collective excitations in low-energy nuclear structure [22, 27], and should serve as a key tool to understand nature of the 0^+ states in nuclei. In particular, in recent years (p,t) and (t,p) experiments have been extensively carried out to identify some new low-lying states in actinide [28–30] and rare-earth [31–36] nuclei. These works suggested that the appearance of a number of excited 0^+ states at low energy, and the structure of the 0^+ excited bands could be interpreted to be, to a large extent, the double octupole phonon coupling. Generally, drawing a robust conclusion about the nature of the 0^+ states and low-lying $K^\pi = 0^+$ bands, however, remains an open question. To address the problem, systematic theoretical studies for nuclear spectroscopy are in order, that are based on a microscopic nuclear structure model.

The interacting boson model (IBM) [37] is among the viable nuclear structure models able to give quantitative descriptions of low-lying states and two-nucleon transfer reactions simultaneously. The IBM has been successfully used for the descriptions of low-energy collective spectra and transition properties in medium-heavy and heavy nuclei. The assumption of the IBM, in its simplest version, is that the collective nucleon pairs with spin and parity $J = 0^+$ and 2^+ are approximated by monopole s and quadrupole d bosons, respectively [37–39]. The application of the IBM to two-nucleon transfers was made initially in Ref. [40]. It has been further applied to study (p,t) and (t,p) two-neutron transfer reactions in the context of the shape QPTs [37, 40–45]. The (p,t) and (t,p) intensities calculated within the model exhibit a phase-transitional, discontinuous change at particular nucleon numbers, and therefore can be identified as signatures of the QPTs. The IBM calculations for the two-neutron transfer intensities were also made to support the interpretation of the 0^+ excited states to be of double-

* nomura@sci.hokudai.ac.jp

octupole phonon states [28–36], in which model parameters were phenomenologically fitted to the observed low-energy spectra.

The present study is aimed to investigate possible effects of octupole correlations on the low-energy 0^+ states and on the relevant two-neutron transfer reactions in the rare-earth region using an updated version of the IBM. In the present work, the Hamiltonian of the IBM is completely determined by means of the constrained self-consistent mean-field (SCMF) calculations [46, 47] based on a given nuclear energy density functional (EDF): The self-consistent calculations provide the potential energy surface (PES) in terms of the relevant shape degrees of freedom, and it is mapped onto the corresponding energy surface in the boson system [48, 49]. This method, hereafter denoted mapped IBM, has been successfully used in a number of nuclear structure (see Ref. [50] and references therein), β-decay [51–53], and double-β-decay studies [54–56]. In particular, the mapped IBM has been extensively used for the spectroscopic calculations for the low-energy quadrupole and octupole collective excitations in a wide range of the nuclear chart [57].

In Ref. [44], the mapped IBM was implemented in the calculations of the (p,t) and (t,p) intensities in the Sm, Gd, and Dy nuclei with the microscopic inputs provided by the Skyrme [58] SkM* [59] EDF. A problem of the IBM mapping revealed in Ref. [44] was that the calculated (p,t) and (t,p) transfer intensities displayed only monotonous changes with the neutron number, which contradicted the empirical data showing a discontinuous change at a particular nucleon number typical of the shape phase transitions. A possible reason for this is that the IBM model space considered in [44] constitutes s and d bosons only. It would be thus of interest to see influences of including the octupole degrees of freedom in the IBM mapping calculations on the systematic of the transfer intensities.

In the present study, the low-energy collective states, (p,t) and (t,p) transfer reactions in the even-even Nd, Sm, and Gd isotopes with $N = 84 - 94$ are specifically considered. These nuclei undergo a rapid nuclear structure change from nearly spherical to strongly deformed shapes near $N = 90$, and have been studied in the IBM as an ideal testing ground for the model. The octupole correlations are expected to play a role in low-lying states in these nuclei, as they are close to the neutron number $N = 88$. In addition, given that the mapped IBM was previously applied to the Gd, Sm [60], and Nd [61] nuclei and provided reasonable descriptions of the low-lying quadrupole and octupole collective states, the ingredients and results of these calculations can be exploited, namely, the IBM Hamiltonian parameters derived from the PES mapping. For the microscopic part, the SCMF calculations were performed in Refs. [60, 61] within the Hartree-Fock-Bogoliubov (HFB) method [62] using the Gogny [63] interaction D1M [64].

The paper is organized as follows. The theoretical framework of the mapped IBM including the formulation of the two-nucleon transfer operators is described in Sec. II. Section III provides results of the mapped IBM calculations for low-energy spectroscopic properties, including the excitation energies and $B(E3)$ values, (p,t) and (t,p) transfer intensities. Section IV is devoted to a summary of the principal results and possible future studies.

II. THEORETICAL PROCEDURE

In the present version of the IBM [37, 65, 66], in addition to s and d bosons, which produce positive-parity states, octupole f bosons, reflecting collective $J = 3^-$ nucleon pairs, should be included to calculate negative-parity states. To keep the discussion simple, the neutron and proton bosons are not distinguished, unlike the previous work of Ref. [44]. The sdf-IBM Hamiltonian takes the form [60, 61];

$$\hat{H} = \epsilon_d \hat{n}_d + \epsilon_f \hat{n}_f + \kappa_2 \hat{Q}_2 \cdot \hat{Q}_2 + \kappa_3 \hat{Q}_3 \cdot \hat{Q}_3 + \rho \hat{L} \cdot \hat{L} \,. \tag{1}$$

The first and second terms, given respectively as $\hat{n}_d = d^\dagger \cdot \tilde{d}$ and $\hat{n}_f = f^\dagger \cdot \tilde{f}$, denote d- and f-boson number operators. The third, fourth, and fifth terms are quadrupole-quadrupole, octupole-octupole, and rotational terms, respectively, with the corresponding operators being

$$\hat{Q}_2 = s^\dagger \tilde{d} + d^\dagger \tilde{s} + \chi_d (d^\dagger \tilde{d})^{(2)} + \chi_f (f^\dagger \tilde{f})^{(2)} \tag{2a}$$

$$\hat{Q}_3 = s^\dagger \tilde{f} + f^\dagger \tilde{s} + \chi_3 (d^\dagger \tilde{f} + f^\dagger \tilde{d})^{(3)} \tag{2b}$$

$$\hat{L} = \sqrt{10} (d^\dagger \tilde{d})^{(1)} + \sqrt{28} (f^\dagger \tilde{f})^{(1)} \,. \tag{2c}$$

The Hamiltonian parameters, ϵ_d, ϵ_f, κ_2, κ_3, ρ, χ_d, χ_f, and χ_3, are determined in such a way [60, 61] that the energy surface of the sdf-IBM, which is provided as the expectation value of the Hamiltonian $\hat{H}$ in the coherent state [67] of s, d, and f bosons, is made to match the Gogny-HFB PES in terms of the axially symmetric quadrupole β_{20} and octupole β_{30} deformations. Further details of the sdf-IBM mapping procedure and derived values of the parameters are found in Refs. [60, 61]. To study the f-boson effects on spectroscopic properties, another set of calculations using the sd-IBM mapping is also carried out, with the corresponding Hamiltonian being of the same form as that in (1), but with those terms involving f bosons omitted.

Within the IBM, the (p,t) and (t,p) transfers are represented by the removal and addition of one boson, respectively, if the boson is treated as a like-particle pair. The present study will be focused on the transfer reactions from the 0^+_1 ground-state state in the initial nucleus to the excited 0^+ states in the final nucleus, hence the angular momenta are unchanged ($\Delta I = 0$). The bosonic operators for the (p,t) and (t,p) transfers are here assumed to be of the forms

$$\hat{P}^{(p,t)} = c_1 \left[\hat{A}(\Omega_\nu, N_\nu) \tilde{s} + c_2 \hat{n}_f \tilde{s} \right] \tag{3}$$

and

$$\hat{P}^{(t,p)} = c_1 \left[s^\dagger \hat{A}(\Omega_\nu, N_\nu) + c_2 s^\dagger \hat{n}_f \right] \ , \tag{4}$$

respectively, where $\hat{P}^{(t,p)} = \left(\hat{P}^{(p,t)}\right)^\dagger$, c_1 and c_2 are parameters. The operator $\hat{A}(\Omega_\nu, N_\nu)$ is defined as [40]

$$\hat{A}(\Omega_\nu, N_\nu) = \left(\Omega_\nu - N_\nu - \frac{N_\nu}{N_\mathrm{B}}\hat{n}_d\right)^{1/2} \left(\frac{N_\nu + 1}{N_\mathrm{B}+1}\right)^{1/2} \tag{5}$$

where Ω_ν denotes the degeneracy of the neutron pairs in a given major shell, and is equal to $(126-82)/2 = 22$ for the nuclei under investigation. N_B is the total number of bosons, and is equal to the number of pairs of valence nucleons [37–39]. N_ν stands for the number of like-neutron bosons, i.e., $1 \leqslant N_\nu \leqslant 6$ for those even-even nuclei with $N = 84, \ldots, 94$, respectively. As is conventional [37], the operator $\hat{n}_d$ in Eq. (5) is replaced with its expectation value in the ground state of the initial nucleus, i.e., $\langle 0^+_{1,i} | \hat{n}_d | 0^+_{1,i} \rangle$. The (p,t) and (t,p) transfer strengths are given as

$$I^{(p,t)}(0^+_i \to 0^+_f) = |\langle N-2, 0^+_f | \hat{P}^{(p,t)} | N, 0^+_i \rangle|^2 \tag{6}$$

$$I^{(t,p)}(0^+_i \to 0^+_f) = |\langle N+2, 0^+_f | \hat{P}^{(t,p)} | N, 0^+_i \rangle|^2 \ . \tag{7}$$

$|N, 0^+_i\rangle$ and $|N \mp 2, 0^+_f\rangle$ stand for the wave functions for the 0^+ states in an initial and a final nuclei with the neutron numbers N and $N \mp 2$ in the (p,t) and (t,p) reactions, respectively. These wave functions are obtained by diagonalizing the mapped *sdf*-IBM Hamiltonian in the boson m-scheme basis [68].

The transfer operators of the forms (3) and (4) are adopted from the (p,t) studies in actinides [28, 29] and in rare-earth (^{166}Er [35] and ^{158}Gd [36]) regions, in which phenomenological calculations using the IBM that consists of the s, d, f, and p (dipole) bosons were carried out. A difference from the transfer operators considered in the *spdf*-IBM calculations is only that the single-p boson term is omitted in the present calculation. These phenomenological *spdf*-IBM calculations suggested that, in addition to the leading order term [the first term in Eq. (3) or Eq. (4)], the transfer operators should include terms involving the negative-parity bosons such as the second term in (3) or (4) to investigate the relevance of the octupole correlations. Unlike most of these empirical IBM studies for the two-nucleon transfers, p bosons are not considered in the present work. The reason for this is not only to avoid complexities, but is also that the microscopic origin of p bosons has not been well established as it is related to a spurious center-of-mass motion [69] and including these degrees of freedom may not be fully justified.

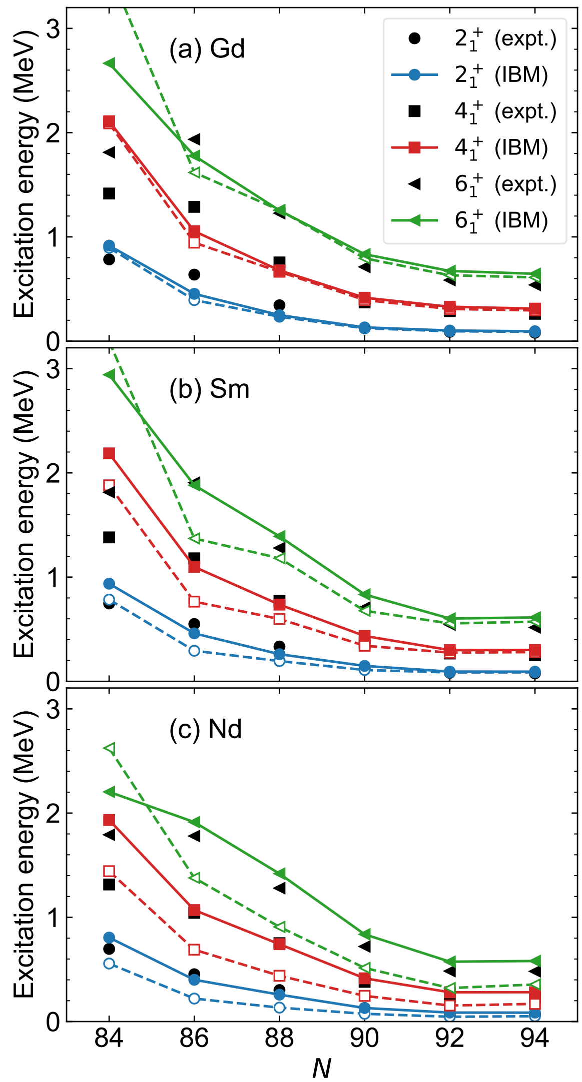

FIG. 1. Calculated excitation energies for the 2^+_1, 4^+_1, and 6^+_1 states for the $^{148-158}$Gd, $^{146-156}$Sm, and $^{144-154}$Nd nuclei within the mapped *sdf*-IBM (solid symbols connected by sold lines) and *sd*-IBM (open symbols connected by dashed lines). Experimental data are adopted from NNDC database [70].

III. RESULTS

A. Low-energy spectroscopy

Figure 1 depicts the 2^+_1, 4^+_1, and 6^+_1 energy levels computed within the mapped *sdf*-IBM and *sd*-IBM. These states constitute the ground-state band, and their decreases with N indicate the increasing quadrupole collectivity. The Gogny-HFB calculations carried out in Refs. [60, 61] suggested the increasing quadrupole β_{20} deformation with a maximal value being approximately 0.33 at $N = 94$. It is seen from Fig. 1(a) that there is no significant difference between the *sdf*-IBM and *sd*-IBM

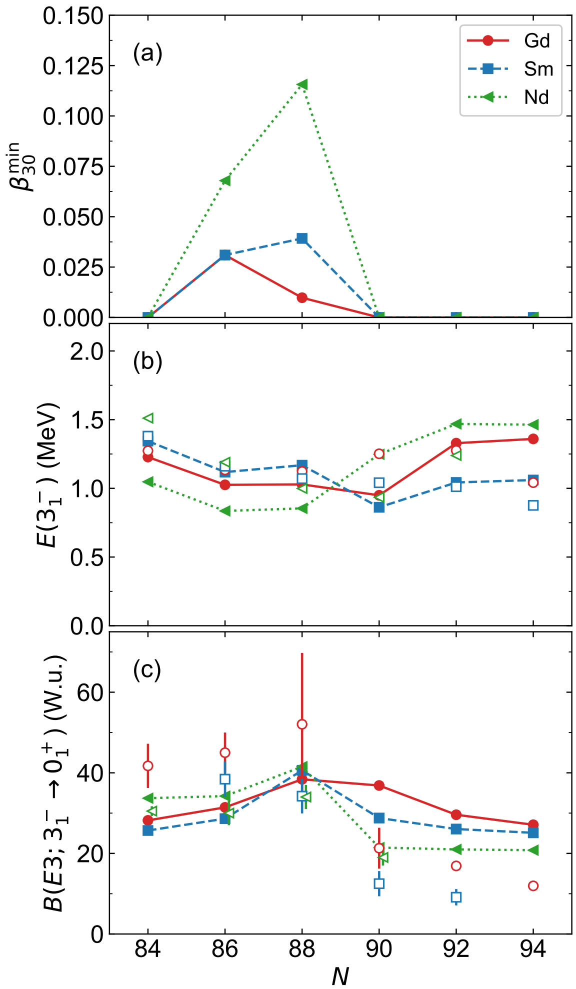

FIG. 2. (a) Octupole deformation $\beta_{30}^{\min}$ corresponding to the energy minimum in the Gogny-HFB (β_{20}, β_{30})-PES, (b) excitation energies $E(3_1^-)$, and (c) $B(E3; 3_1^- \to 0_1^+)$ values for the Gd, Sm, and Nd isotopes resulting from the mapped *sdf*-IBM. Experimental data for the $E(3_1^-)$ and $B(E3; 3_1^- \to 0_1^+)$ values are taken from Refs. [70, 71], and are represented by the open symbols.

results for the Gd isotopes with $N \geqslant 88$, hence the f-boson effects on the ground-state-band levels in Gd do not seem to be crucial. The *sd*-IBM results for the Sm and Nd nuclei, shown in Figs. 1(b) and 1(c), generally suggest lower energy levels than the experimental ones [70]. The *sdf*-IBM provides a higher and, overall, more reasonable description of excitation energies for the yrast states than the *sd*-IBM. The octupole correlation effects on yrast spectra appear to be particularly important in the Sm and Nd isotopes.

Figure 2 shows the calculated octupole deformations, $\beta_{30}^{\min}$, that correspond to the global minima on the Gogny-HFB PESs, and the excitation energies of the 3_1^- state, $E(3_1^-)$, and the $B(E3; 3_1^- \to 0_1^+)$ values, resulting from the *sdf*-IBM. Here the $E3$ operator $\hat{T}^{(E3)}$ is defined as $\hat{T}^{(E3)} = e_3 \hat{Q}_3$, with e_3 and $\hat{Q}_3$ being the effective boson charge and octupole operator of (2b), respectively. In Ref. [61], deformation-dependent e_3 charges of the form

$$e_3 = e_3^0(1 + \overline{\beta_{20}^{\min}}\,\overline{\beta_{30}^{\min}}) \tag{8}$$

were considered for Xe, Ba, Ce, and Nd isotopes. Here $\overline{\beta_{\lambda 0}^{\min}}$ denotes the bosonic quadrupole ($\lambda = 2$) or octupole ($\lambda = 3$) deformation, and is assumed to be proportional to the fermion $\beta_{\lambda 0}$ deformation, $\overline{\beta_{\lambda 0}^{\min}} \equiv C_\lambda \beta_{\lambda 0}^{\min}$, with the constant of proportionality C_λ. e_3^0 is a scale factor constant for an isotopic chain. In the present calculations, the e_3 charges in the above formula (8) are employed also for the Gd and Sm isotopes, and the scale factors $e_3^0 = 0.105$ $e\mathrm{b}^{3/2}$ for the Gd and Sm isotopes, and 0.12 $e\mathrm{b}^{3/2}$ for the Nd isotopes are chosen to reproduce to a good extent the observed $B(E3; 3_1^- \to 0_1^+)$ values.

One sees in Fig. 2(a) that nonzero $\beta_{30}^{\min}$ values are suggested for those nuclei with $N = 86$ and 88, with the maximal octupole deformation being $\beta_{30}^{\min} \approx 0.12$ for ^{148}Nd. For all isotopic chains, the Gogny-HFB calculations suggest that the octupole minimum diminishes for those isotopes with $N \geqslant 90$. However, the PESs for the heavier isotopes are also β_{30} soft [60, 61], and thus suggest that the dynamical octupole correlations may still play a part for the nuclei that are even away from $N = 88$. The calculated $E(3_1^-)$ energies exhibit a weak parabolic behavior with a minimal value at $N = 86$ (Nd) or 90 (Gd and Sm), near which the Gogny-HFB PESs exhibit a $\beta_{30} \neq 0$ minimum or are β_{30} soft. The *sdf*-IBM gives a systematic that is more or less consistent with experiment. The lowering of the observed $E(3_1^-)$ in Gd and Sm from $N = 92$ to 94 indicates that the octupole correlations are still relevant in these heavier isotopes. The present *sdf*-IBM is, however, unable to reproduce this trend, mainly because the Gogny-HFB PESs for the heavier Gd and Sm isotopes with $N \geqslant 90$ do not exhibit a $\beta_{30} \neq 0$ minimum. Even though the Gogny-HFB PESs show certain β_{30} softness for these nuclei, it does not seem to be fully accounted for in the *sdf*-IBM. Note that the $E(3_1^-)$ energies for the ^{144,146,148}Nd nuclei are particularly low. This is because, in these cases, the Gogny-HFB PESs suggest a too pronounced potential valley along the β_{30} deformation. Corresponding to the predicted $E(3_1^-)$ systematic, the reduced transition rates, $B(E3; 3_1^- \to 0_1^+)$, exhibit an inverse parabola with a maximal value at $N \approx 88$, confirming the relevance of octupole collectivity.

Figure 3 compares the excitation energies $E(0_2^+)$ and $E(0_3^+)$ between the *sdf*-IBM and *sd*-IBM. The calculated $E(0_{2,3}^+)$ in the *sd*-IBM are considerably higher than the experimental counterparts by a factor of $2 \sim 4$ particularly for the isotopes with $N \geqslant 90$. The overestimates of the excited 0^+ energy levels are generally encountered in the IBM mapping calculations, and point to certain deficiencies of the model, which arise, e.g., from the restricted boson model space and/or the inputs provided by the EDF self-consistent calculations. The *sdf*-IBM provides lower $0_{2,3}^+$ levels, and reproduces qualitatively

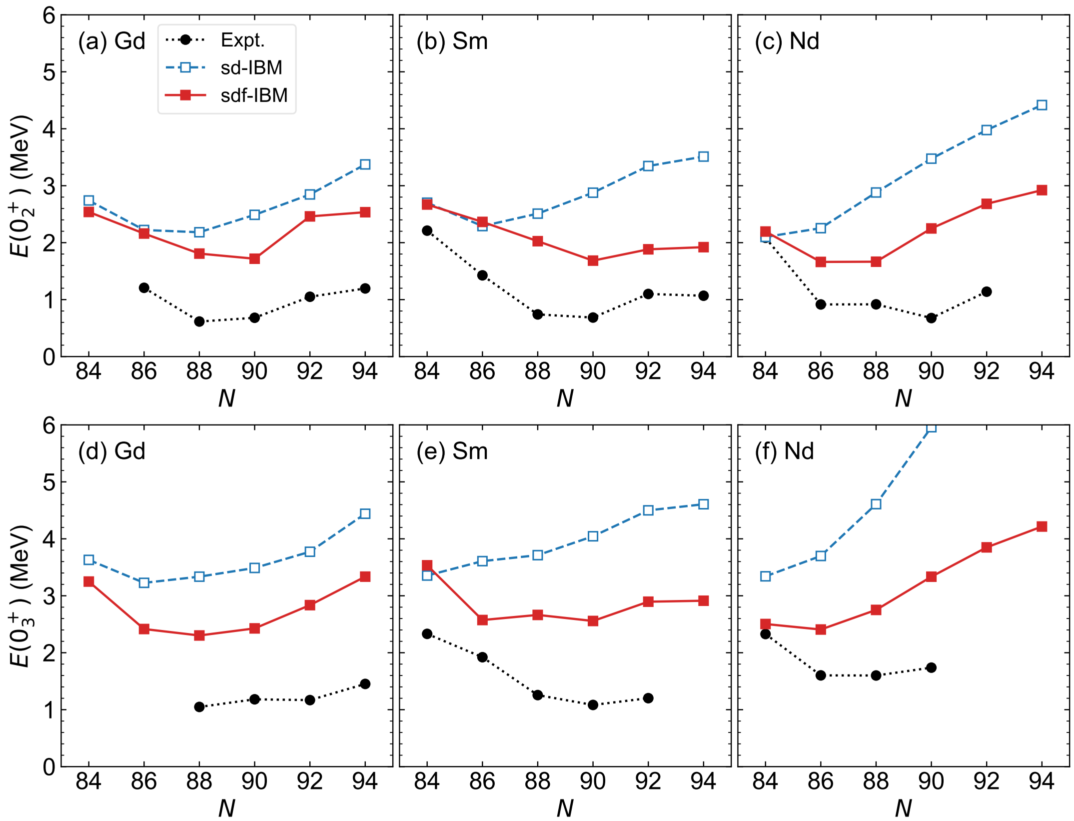

FIG. 3. Calculated 0_2^+ and 0_3^+ energy levels for the Gd, Sm, and Sm isotopes within the mapped *sd*-IBM and *sdf*-IBM in comparison with the experimental data [70].

the observed systematic more reasonably than the *sd*-IBM. It may thus appear that the octupole degrees of freedom could partly account for the lowering of the excited 0^+ energy levels in rare-earth nuclei. However, it should be also noted that the *sdf*-IBM values for $E(0^+_{2,3})$ still overestimate the experimental data, and this implies that some other correlations need to be included in the IBM, such as the configuration mixing, which has been suggested to be important in rare-earth region (see, e.g., Refs. [11, 78, 79]).

Figure 4 exhibits expectation values of the f-boson number operator $\hat{n}_f$ in the lowest three 0^+ states, $\langle \hat{n}_f \rangle_{0^+_n} \equiv \langle 0^+_n | \hat{n}_f | 0^+_n \rangle$, obtained from the mapped *sdf*-IBM. For most of the nuclei, f bosons account for small fractions of the 0^+ ground state as the expectation values are typically calculated to be $\langle \hat{n}_f \rangle_{0^+_1} \approx 0.5$. For the 0^+_2 states, however, $\langle \hat{n}_f \rangle_{0^+_2} \approx 2$ are predicted for most cases, suggesting large octupole contributions. For the Sm and Gd nuclei, a number of the calculated higher-lying 0^+ states in the *sdf*-IBM were shown [60] to have approximately two or even more f bosons in the corresponding wave functions, $\langle \hat{n}_f \rangle_{0^+_n} > 2$. This suggested that octupole degrees of freedom play an important role to explain the existence of a large number of the observed excited 0^+ states in this region. Similar results are obtained for the Nd isotopes. The previous mapped *sdf*-IBM calculations based on the relativistic DD-PC1 EDF [80] and Gogny-D1M EDF [81] also suggested that more than two f bosons are contained in the 0^+_2 states and the corresponding $K^\pi = 0^+_2$ bands in light actinide regions.

Another signature of octupole correlations in a given excited 0^+ state would be the $E3$ transition matrix element $\langle 3^-_1 \| \hat{T}^{(E3)} \| 0^+_{ex} \rangle$, that is comparable in magnitude to that between the 0^+_1 ground state and 3^-_1 state, $\langle 3^-_1 \| \hat{T}^{(E3)} \| 0^+_1 \rangle$. Figure 5 depicts the reduced $E3$ matrix elements, $\langle 3^-_1 \| \hat{T}^{(E3)} \| 0^+_n \rangle$, for the first ($n = 1$), second ($n = 2$), and third ($n = 3$) 0^+ states predicted by the mapped *sdf*-IBM. The $E3$ matrix elements for the ground states, $\langle 3^-_1 \| \hat{T}^{(E3)} \| 0^+_1 \rangle$, are generally largest in each isotopic chain. In many cases, the $\langle 3^-_1 \| \hat{T}^{(E3)} \| 0^+_2 \rangle$ values are calculated to be of the same order of magnitude as, or even larger (for ^{152}Sm and ^{148}Nd) than the $\langle 3^-_1 \| \hat{T}^{(E3)} \| 0^+_1 \rangle$ values, confirming sizable octupole contributions to the 0^+_2 states. The $\langle 3^-_1 \| \hat{T}^{(E3)} \| 0^+_3 \rangle$ matrix elements are, for most of the nuclei, minor in comparison with the $\langle 3^-_1 \| \hat{T}^{(E3)} \| 0^+_1 \rangle$ and $\langle 3^-_1 \| \hat{T}^{(E3)} \| 0^+_2 \rangle$ values. Specifically for ^{152}Gd and ^{150}Sm, $\langle 3^-_1 \| \hat{T}^{(E3)} \| 0^+_3 \rangle$ are pre-

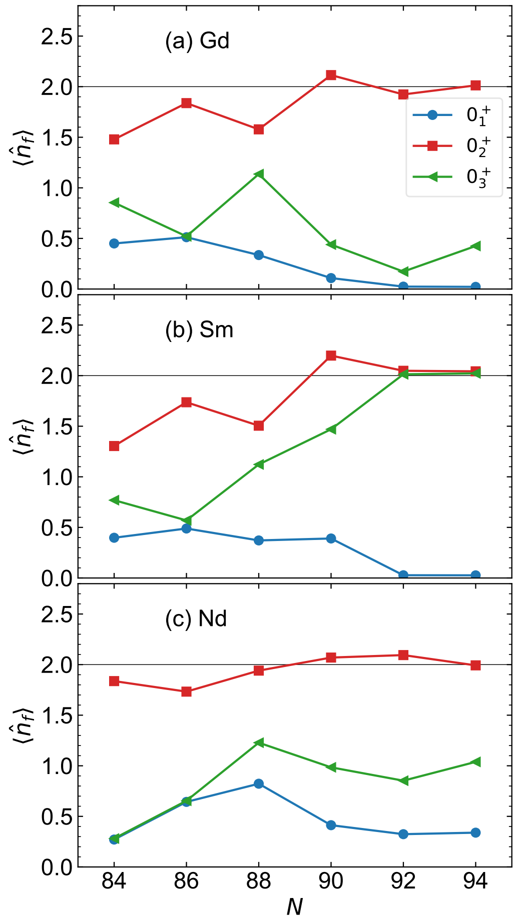

FIG. 4. Expectation values of the f-boson number operator $\langle \hat{n}_f \rangle$ in the 0_1^+, 0_2^+, and 0_3^+ states.

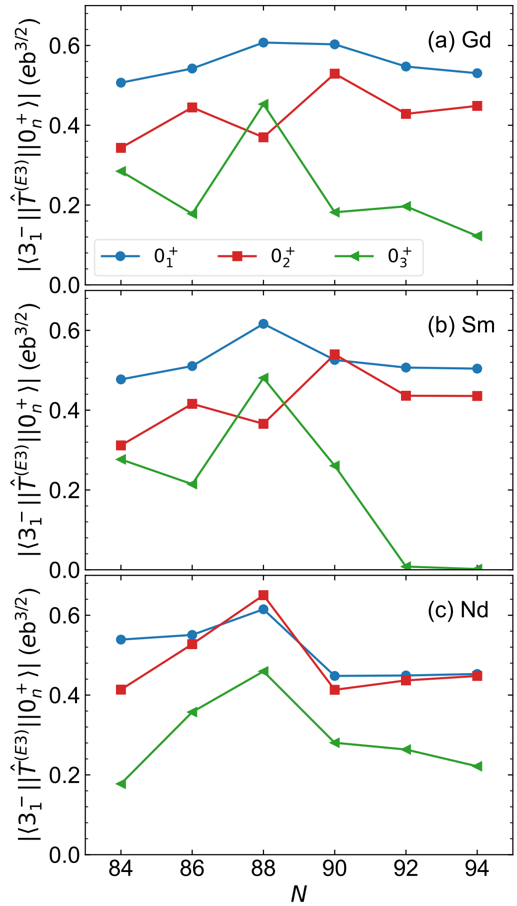

FIG. 5. Absolute values of the calculated reduced matrix elements $|\langle 3_1^- \| \hat{T}^{(E3)} \| 0_n^+ \rangle|$ ($n = 1, 2, 3$) in $e\mathrm{b}^{3/2}$ units.

dicted to be larger than the $\langle 3_1^- \| \hat{T}^{(E3)} \| 0_2^+ \rangle$ values. Since the number of f bosons in the 0_3^+ and 3_1^- states for these nuclei are predicted to be $\langle \hat{n}_f \rangle_{0_3^+} \approx 1$ (Fig. 4), and $\langle \hat{n}_f \rangle_{3_1^-} \approx 1.5$ [61], respectively, such large $\langle 3_1^- \| \hat{T}^{(E3)} \| 0_3^+ \rangle$ matrix elements may have been obtained. What is worth noting is that nearly vanishing $\langle 3_1^- \| \hat{T}^{(E3)} \| 0_3^+ \rangle$ values are obtained for ^{154}Sm and ^{156}Sm, although the 0_3^+ states in these nuclei are similar to the 0_2^+ states in f-boson configuration [cf. Fig. 4(b)]. Probably, it may not be obvious to draw a firm conclusion about the $E3$ properties of the 0_3^+ states solely on the basis of the f-boson content; in fact, the $E3$ strengths $\langle 3_1^- \| \hat{T}^{(E3)} \| 0_3^+ \rangle$ for these deformed Sm nuclei should also be sensitive to the amounts of the d-boson components in the 3_1^- and 0_3^+ states.

B. Two-neutron transfer intensities

By using the sdf-IBM wave functions for each nucleus, the two-neutron transfer intensities defined in Eqs. (6) and (7) are computed. To see effects of the octupole correlations, the following matrix elements are considered:

$$M_s^{(p,t)}(0_1^+ \to 0_n^+) = \langle N-2, 0_n^+ | \tilde{s} | N, 0_1^+ \rangle \tag{9}$$

$$M_{sff}^{(p,t)}(0_1^+ \to 0_n^+) = \langle N-2, 0_n^+ | \hat{n}_f \tilde{s} | N, 0_1^+ \rangle \tag{10}$$

$$M_s^{(t,p)}(0_1^+ \to 0_n^+) = \langle N+2, 0_n^+ | s^\dagger | N, 0_1^+ \rangle \tag{11}$$

$$M_{sff}^{(t,p)}(0_1^+ \to 0_n^+) = \langle N+2, 0_n^+ | s^\dagger \hat{n}_f | N, 0_1^+ \rangle \ . \tag{12}$$

The quantities in Eqs. (9) and (10) [(11) and (12)] correspond to the first and second terms of (p,t) (3) [(t,p) (4)] transfer operators, respectively, up to the coefficients c_1 and c_2, and the factor $\hat{A}_\nu(\Omega_\nu, N_\nu)$. Figures 6, 7, and 8 depict the calculated values of these matrix elements for the Gd, Sm, and Nd isotopes plotted against the excitation energies $E(0_n^+)$ $(n = 1, 2, \dots)$ in the final nuclei.

In all the three isotopic chains, $0_1^+ \to 0_1^+$ transfers are mostly dominated by the s boson terms, that is, the matrix elements $M_s^{(p,t)}(0_1^+ \to 0_1^+)$ and $M_s^{(t,p)}(0_1^+ \to 0_1^+)$ take particularly large values. However, the f-boson terms, represented by $M_{sff}^{(p,t)}(0_1^+ \to 0_1^+)$ and $M_{sff}^{(t,p)}(0_1^+ \to 0_1^+)$, also make sizable contributions in lighter Gd and Sm nuclei with $N \leqslant 88$ and many of the Nd nuclei. Con-

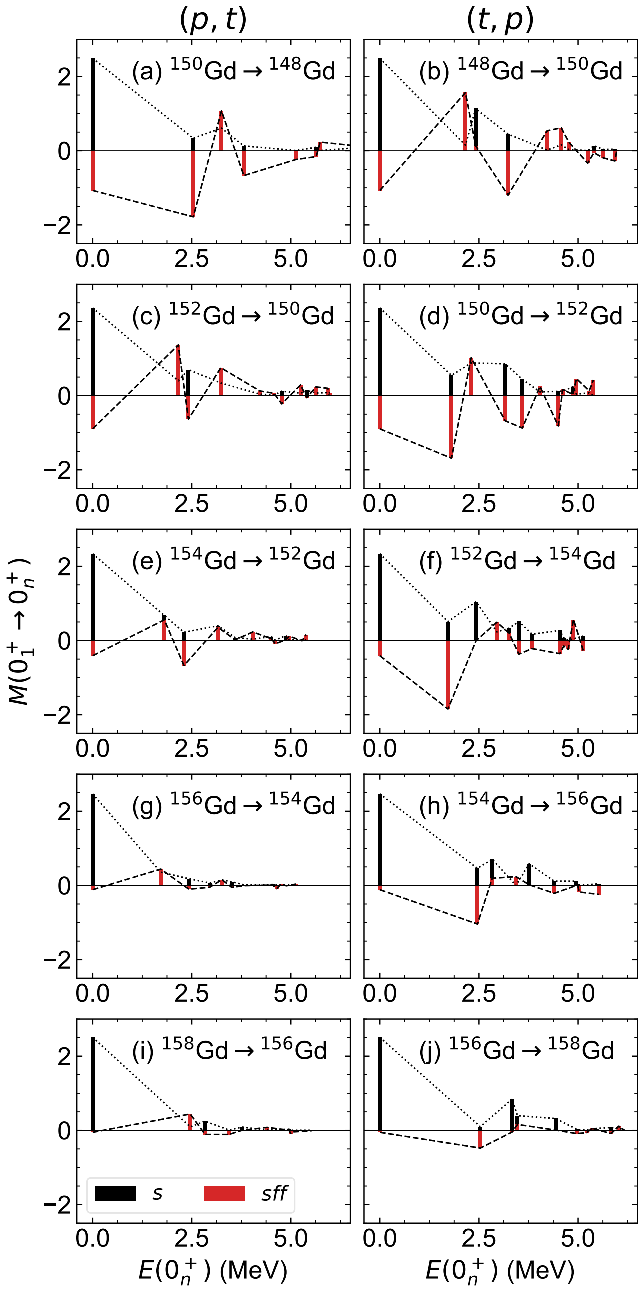

FIG. 6. (Left) Matrix elements $M_{s}^{(p,t)}(0_1^+ \rightarrow 0_n^+)$ and $M_{sff}^{(p,t)}(0_1^+ \rightarrow 0_n^+)$ (denoted "s" and "sff", and connected by dotted and dashed lines, respectively) for the ^{A}Gd$(p,t)^{A-2}$Gd transfer reactions with $A = 150 - 158$ calculated within the mapped *sdf*-IBM. (Right) Matrix elements $M_{s}^{(t,p)}(0_1^+ \rightarrow 0_n^+)$ and $M_{sff}^{(t,p)}(0_1^+ \rightarrow 0_n^+)$ for the ^{A}Gd$(t,p)^{A+2}$Gd reactions with $A = 148 - 156$. In the plot, the sign of the matrix elements $M_{s}^{(p,t)}(0_1^+ \rightarrow 0_n^+)$ $[M_{s}^{(t,p)}(0_1^+ \rightarrow 0_n^+)]$ are made to be positive, with their relative sign to $M_{sff}^{(p,t)}(0_1^+ \rightarrow 0_n^+)$ $[M_{sff}^{(t,p)}(0_1^+ \rightarrow 0_n^+)]$ being unchanged.

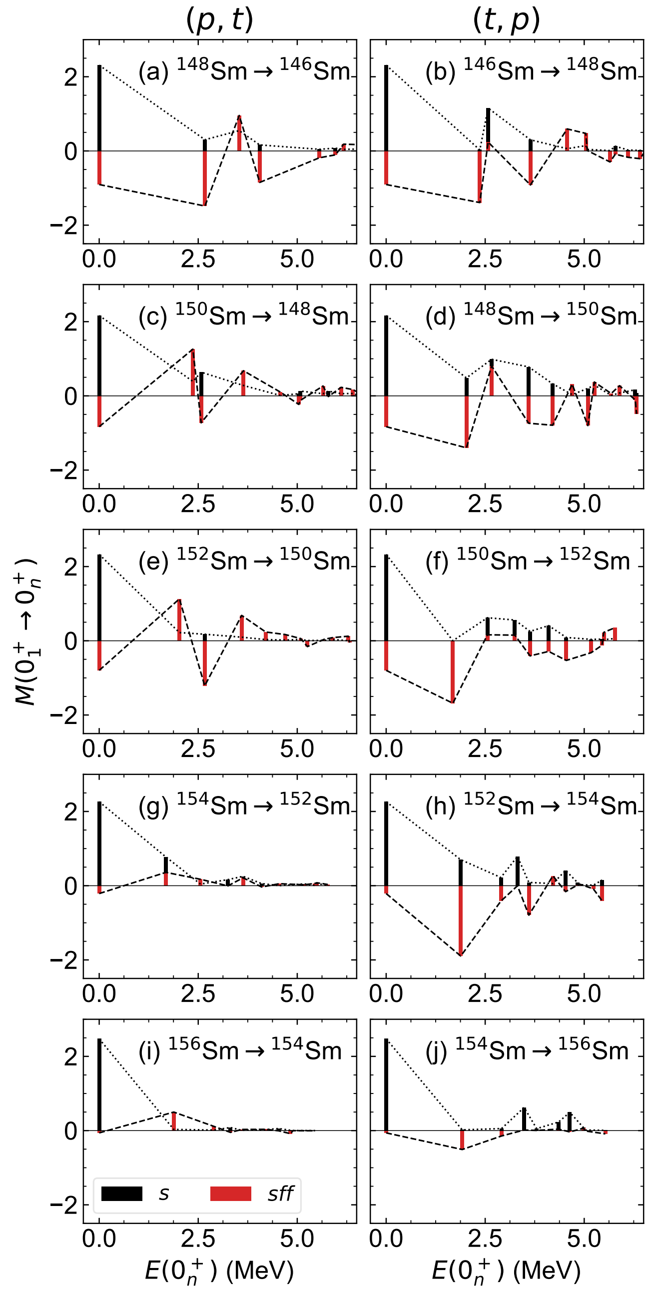

FIG. 7. Same as the caption to Fig. 6, but for the Sm isotopes.

cerning the $0_1^+ \rightarrow 0_{2,3}^+$ transfers, the f-boson contributions, $M_{sff}^{(p,t)}(0_1^+ \rightarrow 0_{2,3}^+)$ and $M_{sff}^{(t,p)}(0_1^+ \rightarrow 0_{2,3}^+)$, are generally quite pronounced with respect to the single s-boson ones, $M_{s}^{(p,t)}(0_1^+ \rightarrow 0_{2,3}^+)$ and $M_{s}^{(t,p)}(0_1^+ \rightarrow 0_{2,3}^+)$. One can indeed see in Figs. 6, 7, and 8 that the corresponding matrix elements $M_{sff}^{(p,t)}(0_1^+ \rightarrow 0_{2,3}^+)$ and $M_{sff}^{(t,p)}(0_1^+ \rightarrow 0_{2,3}^+)$ are much larger in magnitude than $M_{s}^{(p,t)}(0_1^+ \rightarrow 0_{2,3}^+)$ and $M_{s}^{(t,p)}(0_1^+ \rightarrow 0_{2,3}^+)$ in majority of the cases. Corresponding to the results that large fractions of octupole components enter in the 0_2^+ and 0_3^+ states (cf. Fig. 4 and

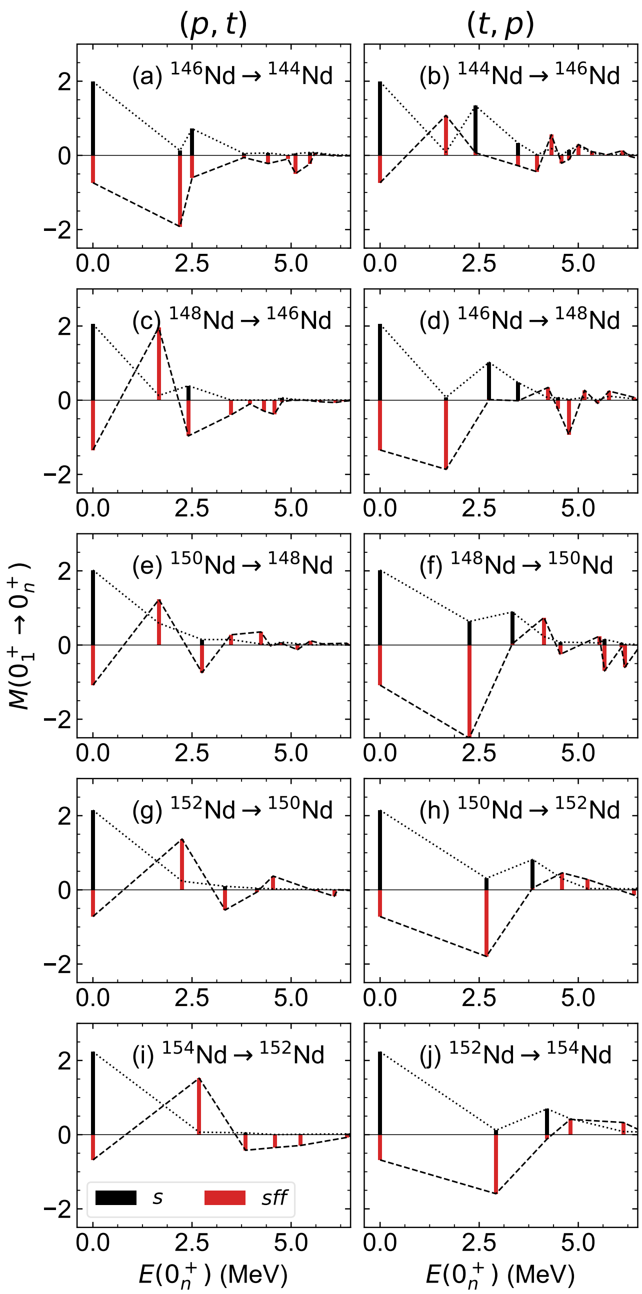

FIG. 8. Same as the caption to Fig. 6, but for the Nd isotopes.

Ref. [60]), the octupole degrees of freedom play a relevant role in the calculations of two-neutron transfer intensities for the $0_1^+ \to 0_{2,3}^+$ reactions. As for those 0_n^+ states higher in energy than 0_3^+, the calculated matrix elements (9)–(12) generally decrease in magnitude, suggesting that the transfers to higher-lying 0^+ states become less significant with increasing excitation energies.

C. Signatures of shape phase transitions

The (p,t) and (t,p) intensities are now computed as signatures of the shape phase transitions, and are compared with the experimental data. As in literature [43], the experimental quantities to be compared with the calculations are those cross sections measured at particular laboratory, θ_{lab}, or center-of-mass, θ_{cm}, angles. According to the results shown in Figs. 6, 7, and 8, the f-boson effects turn out to be pronounced especially for the $0_1^+ \to 0_2^+$ (p,t) and (t,p) transfers for those nuclei with $N \approx 88$ and 90. As shown in Fig. 2(a), the corresponding Gogny-HFB PESs exhibit octupole β_{30} minima. To take these effects into account, the coefficient c_2 is here assumed to depend on the β_{30} deformation and vary with N:

$$c_2 = a + b[\beta_{30}^{\mathrm{min}}(N) + \beta_{30}^{\mathrm{min}}(N \pm 2)]/2 \,, \qquad (13)$$

with "$-$" for (p,t) and "$+$" for (t,p) transfers. In the above formula, a and b are parameters constant for a given isotopic chain and for each of the (p,t) and (t,p) transfers, and the second term represents an average $\beta_{30}^{\mathrm{min}}$ deformation of the two neighboring isotopes. The a and b values are chosen so as to reasonably reproduce the overall behaviors of experimental transfer intensities with N. The remaining parameter, c_1 [(3) and (4)], is an overall scale factor, and is determined so that the transfer intensities should be of the same order of magnitude as the experimental values. The adopted values of the parameters c_1, a, and b are summarized in Table I, and the resultant c_2 values are shown in Table II. One can observe in Table II that the c_2 values vary appreciably at $N \approx 88$, and take a large negative value for the $N = 88 \to 86$ (p,t) and $N = 86 \to 88$ (t,p) transfers.

TABLE I. Adopted values of the parameters for the transfer operators in the *sdf*-IBM, see Eqs. (6) and (7).

	Gd		Sm		Nd	
	(p,t)	(t,p)	(p,t)	(t,p)	(p,t)	(t,p)
c_1	3.9	2.5	3.9	2.8	4.7	2.3
a	4	3.5	1	1	1.5	1
b	−200	−250	−150	−100	−25	−30

To study f-boson effects quantitatively, the *sd*-IBM mapping calculations for the $I^{(p,t)}(0_1^+ \to 0_{1,2}^+)$ and $I^{(t,p)}(0_1^+ \to 0_{1,2}^+)$ values are also performed. For these calculations the same values of the parameter c_1 as those for the *sdf*-IBM (cf. Table I) are adopted.

Furthermore, the mapped *sdf*-IBM and *sd*-IBM results are compared with those obtained from purely phenomenological *sd*-IBM calculations in Ref. [43], in which the Hamiltonian in the so-called consistent-Q formalism (CQF) [82], suitable for studying the shape QPTs, was

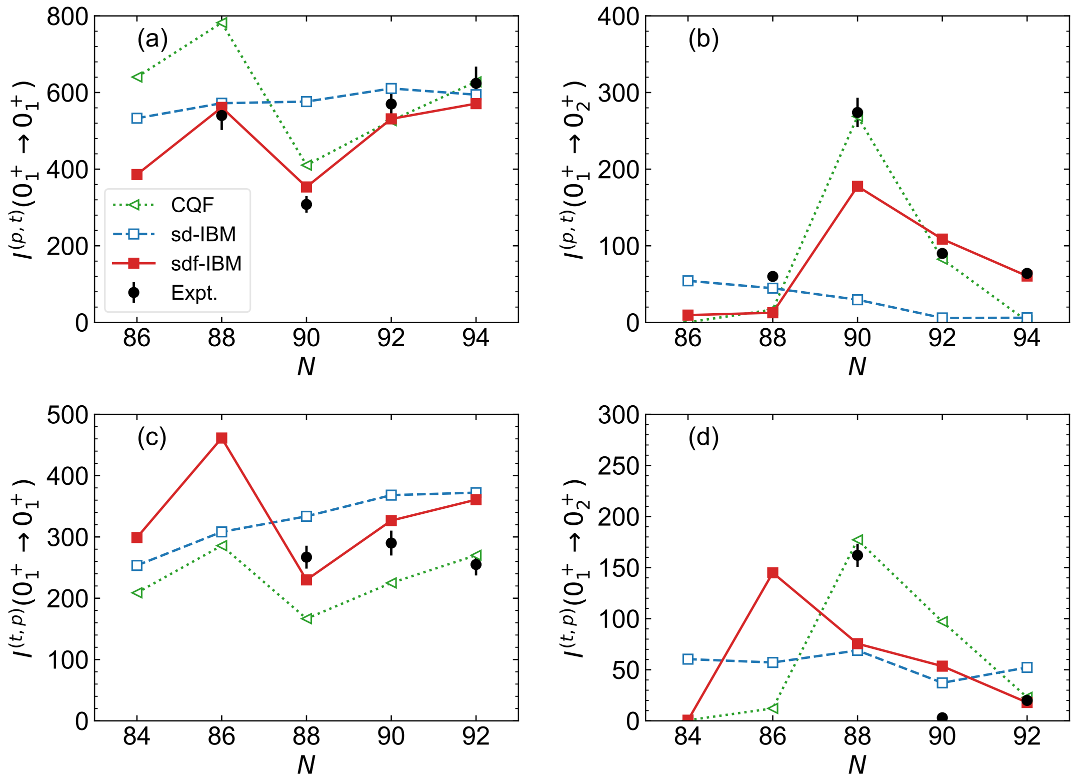

FIG. 9. (p,t) and (t,p) transfer intensities for the $0_1^+ \to 0_1^+$ and $0_1^+ \to 0_2^+$ transitions in the Gd isotopes plotted as functions of the neutron number N of the initial nucleus. Calculations are made within the mapped *sdf*-IBM and *sd*-IBM, and phenomenological *sd*-IBM using the CQF Hamiltonian. Experimental data included are differential cross sections (in μb/sr units) measured at the laboratory angle $\theta_{\mathrm{lab}} = 30^\circ$ for the ${}^{A}\mathrm{Gd}(p,t)^{A-2}\mathrm{Gd}$ [72], and ${}^{A}\mathrm{Gd}(t,p)^{A+2}\mathrm{Gd}$ [73, 74] reactions.

considered:

$$\hat{H}_{\mathrm{CQF}} = \epsilon_0 \left[(1-\eta)\hat{n}_d - \frac{\eta}{4N_{\mathrm{B}}} \hat{Q}^{\chi} \cdot \hat{Q}^{\chi} \right] . \tag{14}$$

ϵ_0 is an overall scale factor usually adjusted to reproduce the experimental energy levels in each nucleus, η is a control parameter, and the operator $\hat{Q}^{\chi}$ is the quadrupole operator in the *sd*-IBM with χ being the parameter for the $(d^\dagger \tilde{d})^{(2)}$ term. The values of the ϵ_0, η, and χ parameters are adopted from Tables I, II, and III of Ref. [43]. As shown in Ref. [43], the IBM-CQF fitting calculations provide excellent phenomenological descriptions of the experimental low-energy spectra of the positive-parity yrast states and excited 0^+ states in rare-earth region.

TABLE II. Values of the neutron-number-dependent coefficients c_2 (13) used for the (p,t) and (t,p) transfer operators for the considered Gd, Sm, and Nd nuclei.

	Gd		Sm		Nd	
N	(p,t)	(t,p)	(p,t)	(t,p)	(p,t)	(t,p)
84		−0.37		−0.55		−0.02
86	0.90	−1.60	−1.32	−2.51	0.65	−1.75
88	−0.08	2.28	−4.26	−0.96	−0.79	−0.73
90	3.02	3.50	−1.94	1.00	0.05	1.00
92	4.00	3.50	1.00	1.00	1.50	1.00
94	4.00		1.00		1.50	

Figures 9, 10, and 11 show the calculated $I^{(p,t)}(0_1^+ \to 0_{1,2}^+)$ and $I^{(t,p)}(0_1^+ \to 0_{1,2}^+)$ intensities in the Nd, Sm, and Gd isotopes. Experimental data are adopted from Refs. [73–77]. Some more details about the data are given in the captions to Figs. 9, 10, and 11. One can see from Fig. 9(a) that the calculated $I^{(p,t)}(0_1^+ \to 0_1^+)$ value for Gd in the *sdf*-IBM exhibits a discontinuous change from $N = 88-90$. This systematic resembles that obtained in the IBM-CQF calculation, and is considered to be a signature of the shape phase transition. Algebraic relations in the IBM suggest that, in the large-boson-number limit ($N_{\mathrm{B}} \to \infty$), the $0_1^+ \to 0_1^+$ two-neutron transfer intensities, $|\langle N, 0_1^+|s|N+2, 0_1^+\rangle|^2$, are proportional to $N_{\mathrm{B}}+1$ and $(N_{\mathrm{B}}+1)(2N_{\mathrm{B}}+3)/3(2N_{\mathrm{B}}+1)$ in the U(5) (vibrational) and SU(3) (rotational) limits, respectively [37, 40]. In the IBM-CQF, the phase-transitional behavior of $I^{(p,t)}(0_1^+ \to 0_1^+)$ is reproduced solely with the s and d boson degrees of freedom, using only the overall scale factor c_1 in (3) and (4) for the transfer operators.

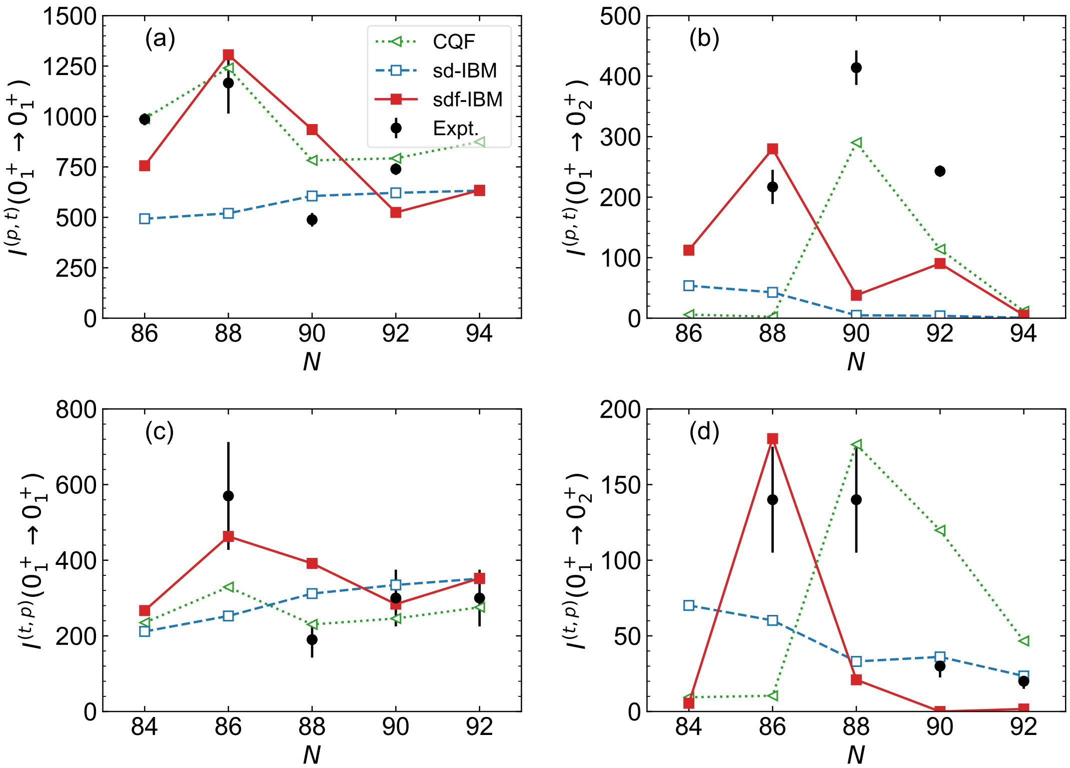

FIG. 10. Same as the caption to Fig. 9, but for the Sm isotopic chain. Experimental data for the (p,t) and (t,p) transfers are taken from Refs. [75, 76], corresponding to the laboratory angle $\theta_{\mathrm{lab}} = 25^{\circ}$ and center-of-mass angle $\theta_{\mathrm{cm}} = 27.8^{\circ}$, respectively.

In the EDF-mapped *sd*-IBM, however, such an abrupt change of the transfer intensities cannot be produced, provided that the transfer operators are of the present forms consisting only of the term proportional to s and $s^{\dagger}$ operators.

In Fig. 9(b) the predicted $I^{(p,t)}(0_1^+ \rightarrow 0_2^+)$ value in the mapped *sdf*-IBM exhibits a kink at $N = 90$, similarly to the IBM-CQF values. Note that the selection rules of the IBM with the $N_{\mathrm{B}} \rightarrow \infty$ limit do not allow the $0_1^+ \rightarrow 0_2^+$ (p,t) transitions in both the U(5) and SU(3) limits. However, as seen from Fig. 9(b), all the present IBM calculations give finite $I^{(p,t)}(0_1^+ \rightarrow 0_2^+)$ values. These deviations may suggest that the group theoretical argument does not hold concerning the $I^{(p,t)}(0_1^+ \rightarrow 0_2^+)$ intensity, as the symmetries are supposed to be broken and certain degrees of configuration mixing are likely to take place in realistic (numerical) IBM calculations. Experimental (p,t) data for the Gd nuclei and those for the neighboring Sm [Fig. 10(b)] also suggest large $I^{(p,t)}(0_1^+ \rightarrow 0_2^+)$ values.

The $I^{(t,p)}(0_1^+ \rightarrow 0_1^+)$ values, displayed in Fig. 9(c), exhibit a quite similar N-dependence to $I^{(p,t)}(0_1^+ \rightarrow 0_1^+)$ values. The $0_1^+ \rightarrow 0_1^+$ (t,p) transfers are allowed by the selection rules in the IBM with $N_{\mathrm{B}} \rightarrow \infty$ [40], and the same symmetry limits can be used to interpret the change of $I^{(p,t)}(0_1^+ \rightarrow 0_1^+)$ from $N = 86 - 88$ as the U(5)-SU(3) phase transition. In Fig. 9(d), the $I^{(t,p)}(0_1^+ \rightarrow 0_2^+)$ intensities calculated in the IBM-CQF show a similar systematic to the $I^{(p,t)}(0_1^+ \rightarrow 0_2^+)$ one, that is, the former is peaked at $N = 88$ and the latter at $N = 90$. The *sdf*-IBM also gives a maximal $I^{(t,p)}(0_1^+ \rightarrow 0_2^+)$ value at $N = 86$, exhibiting a certain similarity in tendency to the $I^{(p,t)}(0_1^+ \rightarrow 0_2^+)$ value. The results of the three sets of the IBM calculations that the $I^{(t,p)}(0_1^+ \rightarrow 0_2^+)$ intensity is enhanced for deformed or transitional nuclei are more or less consistent with the symmetry argument in the IBM: The matrix element $|\langle N+2, 0_2^+|s^{\dagger}|N, 0_1^+\rangle|^2$ vanishes in the U(5) limit, but is finite in the SU(3) limit [40].

The calculated $I^{(p,t)}(0_1^+ \rightarrow 0_1^+)$ values in the *sdf*-IBM for Sm isotopes, shown in Fig. 10(a), exhibit a pattern that signals the nearly-spherical-to-deformed shape phase transition, as in the case of the Gd isotopes. This result is also overall consistent with the experimental data and with the IBM-CQF fitting calculation, apart from the discrepancy in systematic from $N = 90 - 92$. Figure 10(b) shows that the *sdf*-IBM gives the largest $I^{(p,t)}(0_1^+ \rightarrow 0_2^+)$ intensity at $N = 88$, whereas the IBM-CQF phenomenology gives a vanishing $I^{(p,t)}(0_1^+ \rightarrow 0_2^+)$ intensity at $N = 88$. The experimental and IBM-CQF $I^{(p,t)}(0_1^+ \rightarrow 0_2^+)$, however, become maximal at $N = 90$. The discrepancy may be accounted for by the fact that the employed bosonic transfer operators in (3) and (4) are of too simplified forms to reproduce all details of the empirical trends of the transfer intensities, or the chosen

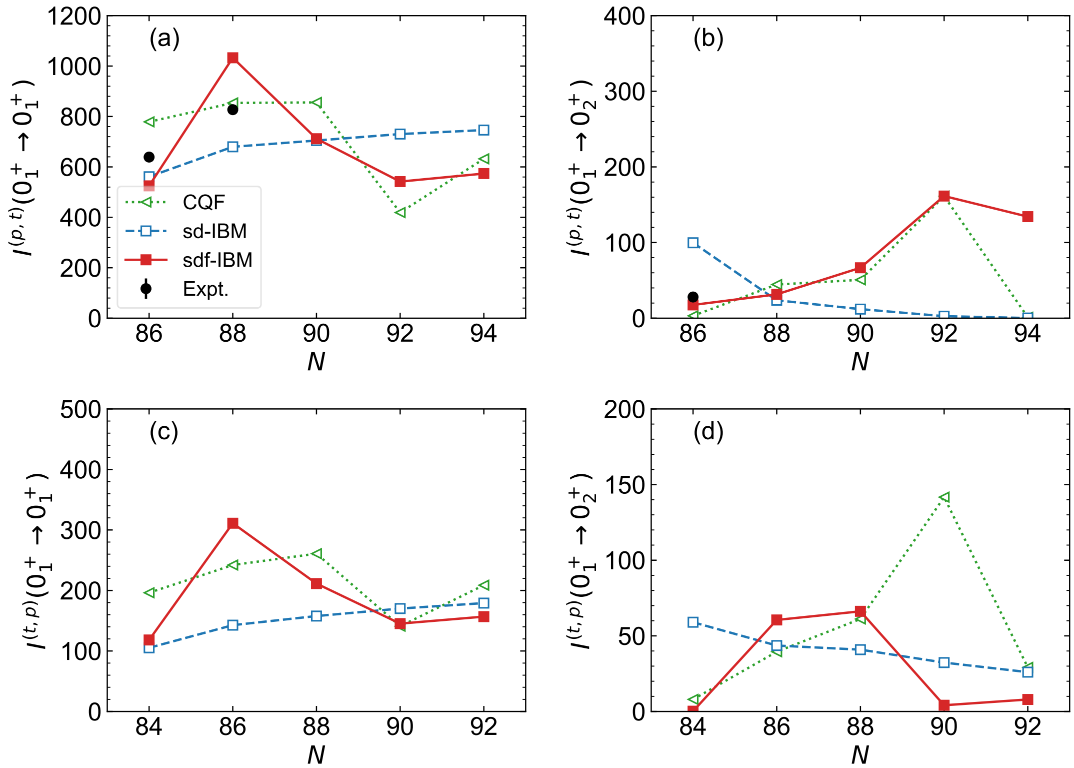

FIG. 11. Same as the caption to Fig. 9, but for the Nd isotopic chain. Experimental data for the (p,t) transfers are adopted from Ref. [77], corresponding to the angle $\theta_{\rm lab} = 10°$.

parameters for the operators might not be optimal. In Fig. 10(c), the experimental data for the $I^{(t,p)}(0_1^+ \to 0_1^+)$ intensities appear to show a behavior similar to that of the $I^{(p,t)}(0_1^+ \to 0_1^+)$ ones. Both the mapped *sdf*-IBM and IBM-CQF overall reproduce this systematic. As one can see in Fig. 10(d), the mapped *sdf*-IBM predicts for $I^{(t,p)}(0_1^+ \to 0_2^+)$ value to be peaked at $N = 86$, and this value is within error bar of the experimental value [76].

As one can see from Fig. 11, basically similar observations can apply to the Nd isotopic chain. The $I^{(p,t)}(0_1^+ \to 0_{1,2}^+)$ data are scarce and only the relative intensities of $I^{(t,p)}(0_1^+ \to 0_2^+)$ to $I^{(t,p)}(0_1^+ \to 0_1^+)$ are known experimentally for the ^{144}Nd$(t,p)^{146}$Nd, ^{146}Nd$(t,p)^{148}$Nd, ^{148}Nd$(t,p)^{150}$Nd, and ^{150}Nd$(t,p)^{152}$Nd transfer reactions [83]. The a and b parameters (13) for the Nd isotopes are thus determined so as to be similar in tendency to the $I^{(p,t)}(0_1^+ \to 0_{1,2}^+)$ values computed by the IBM-CQF. For the IBM-CQF values of $I^{(p,t)}(0_1^+ \to 0_{1,2}^+)$ shown in Figs. 11(a) and 11(b) the c_1 value of 5.48 considered in Ref. [43] is here modified as $c_1 = 4.0$. In addition, to compute the $I^{(t,p)}(0_1^+ \to 0_{1,2}^+)$ intensities, plotted in Figs. 11(c) and 11(d), the same c_1 parameter as that for the Gd isotopes, $c_1 = 2.24$ [43], is employed. The measured $I^{(t,p)}(0_1^+ \to 0_2^+)/I^{(t,p)}(0_1^+ \to 0_1^+)$ ratios for the four reactions are 0.09, 0.15, 1.28, and 0.72, respectively, obtained with the center-of-mass angles $\theta_{\rm cm} = 20.2°$, $27.8°$, $27.8°$, and $27.8°$. These data suggest the largest $I^{(t,p)}(0_1^+ \to 0_2^+)/I^{(t,p)}(0_1^+ \to 0_1^+)$ ratio for the ^{148}Nd$(t,p)^{150}$Nd reaction, and this systematic is qualitatively reproduced in the present *sdf*-IBM calculation, yielding the ratios 0.002, 0.19, 0.31, 0.03, respectively.

D. Transfer intensity distributions

In Figs. 12 and 13, calculated $I^{(p,t)}(0_1^+ \to 0_n^+)$ and $I^{(t,p)}(0_1^+ \to 0_n^+)$ transfer intensities within the mapped *sdf*-IBM are compared with the corresponding quantities obtained from the mapped *sd*-IBM and IBM-CQF. For the *sdf*-IBM, the a and b parameters given in Table I are used. The overall scale factor c_1 for all the three sets of the IBM calculations is assumed to be $c_1 = 0.1$, in order to facilitate the comparisons. It is also noted that only the calculated results for Gd isotopes are discussed, since the corresponding results for the Sm and Nd isotopes turn out be similar.

In Fig. 12, the $I^{(p,t)}(0_1^+ \to 0_1^+)$ values obtained from the *sdf*-IBM for the (p,t) transfers of the Gd isotopes are all larger than those in the *sd*-IBM and IBM-CQF by an order of magnitude. The $I^{(p,t)}(0_1^+ \to 0_{2,3}^+)$ values for the transitional nuclei near $N = 88$ (^{152}Gd) and 90

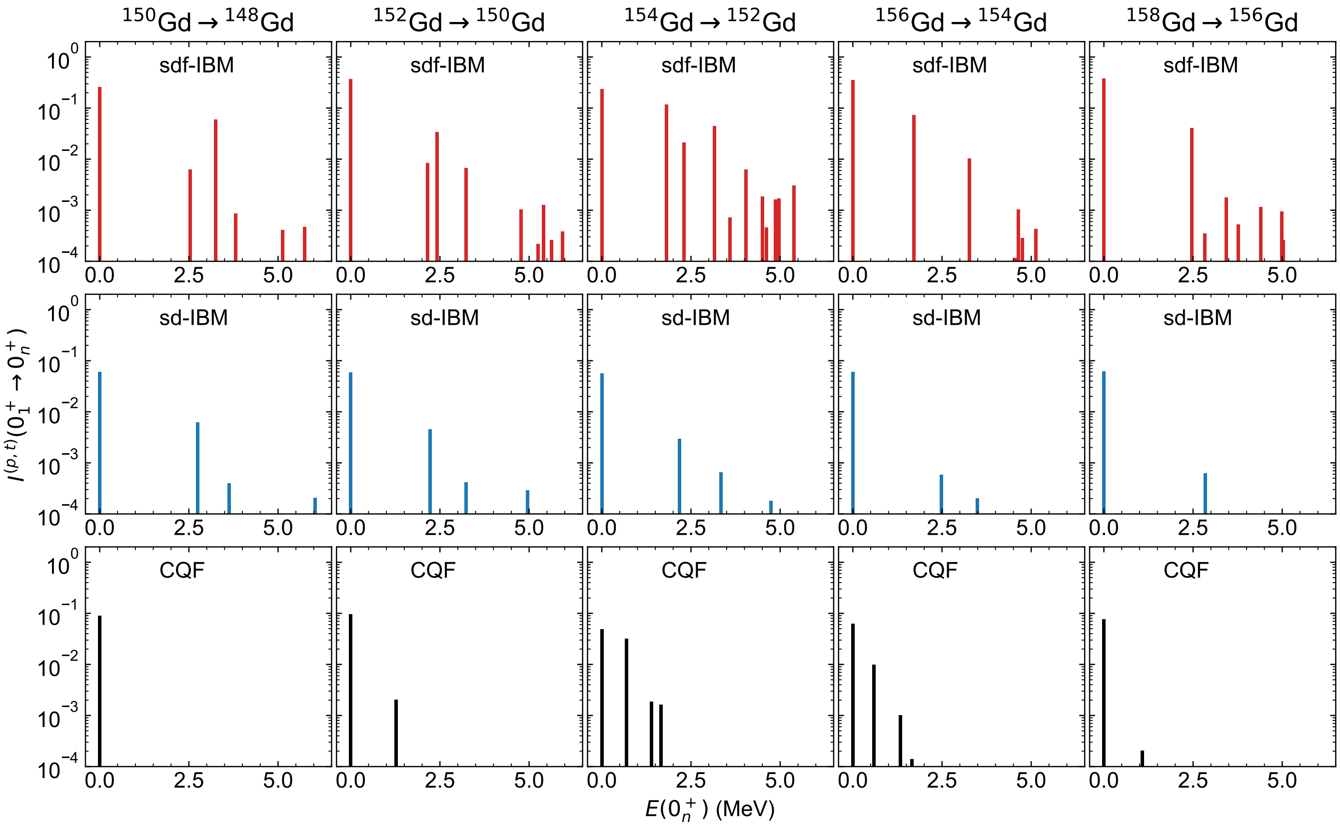

FIG. 12. Predicted (p,t) transfer intensities $I^{(p,t)}(0_1^+ \to 0_n^+)$ from the *sdf*-IBM, *sd*-IBM, and IBM-CQF calculations for the Gd isotopes. The adopted parameters for the (p,t) operators are given in Table I, but the c_1 values are replaced with a dimensionless value $c_1 = 0.1$ for all the three IBM calculations.

(^{154}Gd) are predicted to be larger in the *sdf*-IBM than in the *sd*-IBM by orders of magnitude. Also a large number of excited 0^+ are predicted in the *sdf*-IBM within the considered energy range of up to 6.5 MeV. In both the *sdf*-IBM and *sd*-IBM, the (p,t) intensities are mostly accounted for by the $0_1^+ \to 0_1^+$ transfers and, especially in the *sd*-IBM, the contributions from the higher-lying 0^+ states are considerably minor. In the IBM-CQF calculations, the excited 0^+ states are generally predicted to be much lower in energy than those in the *sdf*-IBM and *sd*-IBM mapping results. As pointed out earlier, the overestimates of the 0_2^+ and 0_3^+ energies in the mapped IBM calculations imply certain missing correlations, and necessitate further refinements of the methodology. Similarly to the two sets of the mapped IBM calculations, the IBM-CQF suggests that the $0_1^+ \to 0_1^+$ (p,t) transfers are dominant, and the (p,t) transfers to higher-lying 0^+ states are essentially negligibly small.

Similar observations seem to hold for the systematic of the $I^{(t,p)}(0_1^+ \to 0_n^+)$ intensities. In Fig. 13 there are also significant differences in the $I^{(t,p)}(0_1^+ \to 0_1^+)$ values between the *sdf* and *sd* boson models. The (t,p) transfer to the 0_2^+ state in the ^{150}Gd nucleus is particularly strong within the *sdf*-IBM, which is of the same order of magnitude as the $I^{(t,p)}(0_1^+ \to 0_1^+)$ transfer intensity. In the *sdf*-IBM, large (t,p) strengths to the higher-lying 0^+ states are obtained for the ^{150}Gd$(t,p)^{152}$Gd and ^{152}Gd$(t,p)^{154}$Gd transfer reactions.

IV. CONCLUSIONS

Influences of the octupole degrees of freedom on the two-neutron transfer reactions and properties of excited 0^+ states in rare-earth nuclei have been investigated in terms of the *sdf*-IBM that is based on the nuclear EDF. In this framework, the strength parameters for the *sdf*-IBM Hamiltonian were obtained by mapping the axially symmetric quadrupole-octupole energy surface calculated by the constrained Gogny-EDF HFB method onto the expectation value of the boson Hamiltonian in the intrinsic state. Resulting *sdf*-IBM wave functions for the initial- and final-state nuclei were used to calculate intensities of the (p,t) and (t,p) transfers between 0^+ states.

While f bosons are essential building blocks to compute negative-parity states, these degrees of freedom have been shown to play a role in low-lying positive-parity

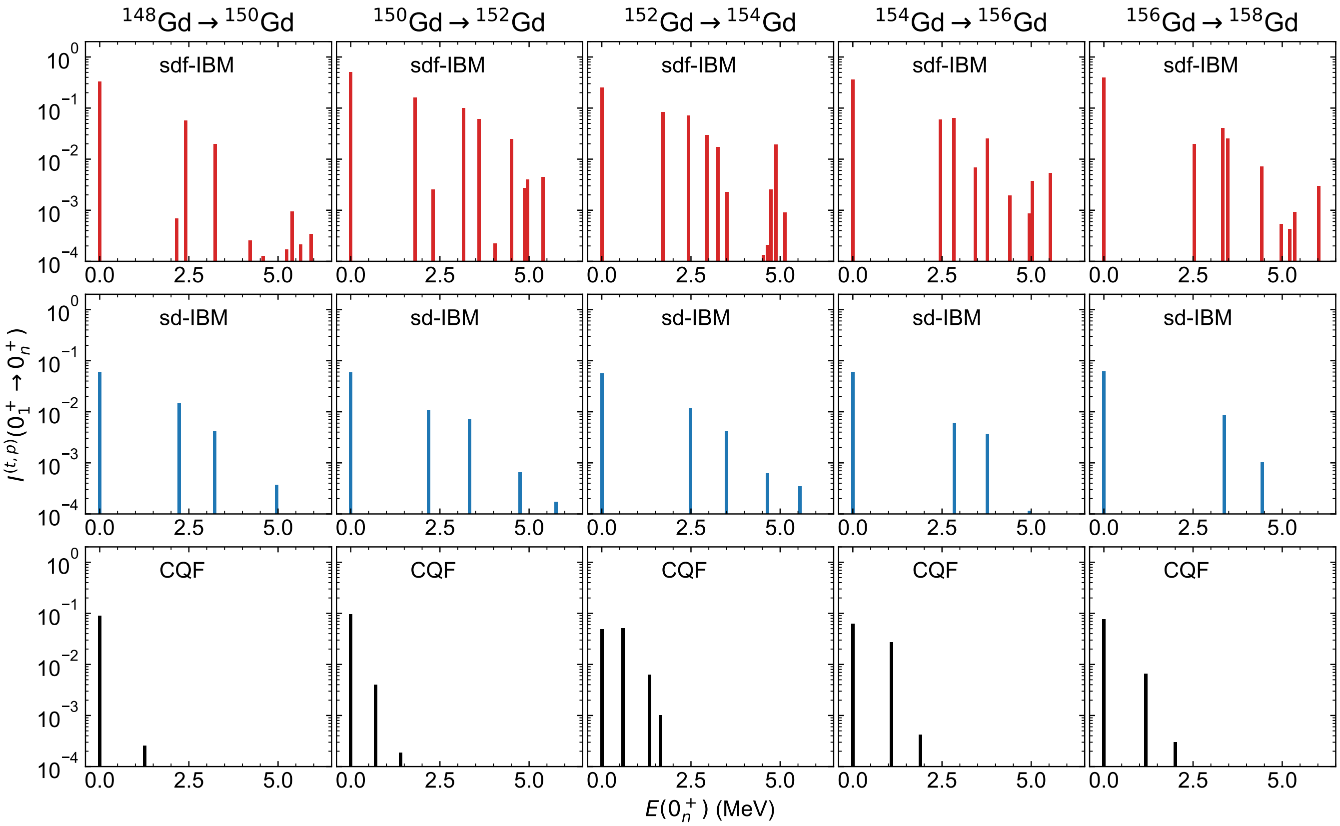

FIG. 13. Same as the caption to Fig. 12, but for the (t,p) transfer reactions.

states, including the $0_{2,3}^+$ energy levels. The mapped *sdf*-IBM calculations suggested that the 0_2^+ states in almost all the considered rare-earth nuclei are accounted for by the presence of f-boson components, with the expectation values typically $\langle \hat{n}_f \rangle_{0_2^+} \approx 2$, and that even the 0_1^+ ground states in these nuclei contain certain amounts of the f-boson components. As compared with the *sd*-IBM, a large number of the excited 0^+ states are produced in the *sdf*-IBM, many of which were shown to be characterized by more than two f-boson content. However, it should be also noted that the calculated $0_{2,3}^+$ levels in the *sdf*-IBM turned out to be still much higher than the experimental ones, and some other degrees of freedom, such as the configuration mixing of normal and intruder states, and the dynamical pairing deformations would need to be taken into account.

For the $0_1^+ \to 0_1^+$ transfer reactions, the calculated matrix elements of the leading-order term in the transfer operator proportional to $s^{(\dagger)}$ have been shown to be considerably larger than those of the second term of the form $\hat{n}_f s^{(\dagger)}$. However, the $0_1^+ \to 0_{2,3}^+$ (p,t) and (t,p) matrix elements of the $\hat{n}_f s^{(\dagger)}$ term, particularly for the nuclei with $N = 88$ or 90, have been shown to be of the same order of magnitude as or even larger than those of the single s-boson $[s^{(\dagger)}]$ term. The resultant transfer intensities, $I^{(p,t)}(0_1^+ \to 0_{1,2}^+)$ and $I^{(t,p)}(0_1^+ \to 0_{1,2}^+)$, were compared with the experimental data and with those values obtained from the mapped *sd*-IBM and phenomenological *sd*-IBM calculations. The behavior of the (p,t) and (t,p) transfer intensities are considered to be empirical signatures of the shape QPT from the nearly spherical to strongly deformed states in rare-earth region. By assuming nucleon-number- and deformation-dependent parameters for the transfer operators, the mapped *sdf*-IBM reproduced the decreasing patterns of the $I^{(p,t)}(0_1^+ \to 0_{1,2}^+)$ and $I^{(t,p)}(0_1^+ \to 0_{1,2}^+)$ intensities near $N = 88$ or 90. These results are consistent with the experimental data and with the IBM-CQF fitting calculations. In the EDF-mapped IBM framework, the consideration of only the s and d boson degrees of freedom turned out to be insufficient to produce a discrete change of the transfer intensities, and the inclusion of f bosons appears to efficiently account for such systematic.

The present work suggests the relevance of octupole correlations to predicting two-neutron transfers, to interpretation of the excited 0^+ states in terms of the multi-octupole-phonon configurations, and to the shape QPTs starting from the microscopic EDF calculations. A possible future work is the extension of the analysis to the (p,t) and (t,p) studies in the light actinide region, for which updated experimental results have been recently reported. Also in this region, a permanent octupole deformation was empirically suggested in a few nuclei, and a similar type of the nearly-spherical-to-axially-deformed shape phase transitions to those in the rare-earth region are observed. It would also be of interest to assess and improve the accuracy of the theoretical method, since, for instance, the transfer operator considered in this work is of a simplified form, and higher-order terms may quantitatively change the results and influence conclusions. In particular, given that the IBM-CQF, involving only s and d bosons, can reproduce the phase-transitional behaviors of the two-nucleon transfer intensities, the mapped sd-IBM that includes such high-order contributions in the transfer operators may be able to reproduce the systematic of the transfer intensities without including f bosons. It would be an interesting future study to investigate further the roles played by the f boson degrees of freedom in the nuclear phenomena related to the excited 0^+ states in deformed heavy nuclei within the mapped IBM In addition, given the important roles played by the configuration mixing of intrinsic shapes in the rare-earth region, an extension of the IBM mapping procedure to incorporate mixing in the formalism will be another interesting future study.

ACKNOWLEDGMENTS

This work has been supported by JSPS KAKENHI Grant No. JP25K07293.

[1] I. Ahmad and P. A. Butler, Annu. Rev. Nucl. Part. Sci. **43**, 71 (1993).
[2] P. A. Butler and W. Nazarewicz, Rev. Mod. Phys. **68**, 349 (1996).
[3] P. A. Butler, J. Phys. G: Nucl. Part. Phys. **43**, 073002 (2016).
[4] P. A. Butler, Proc. R. Soc. A **476**, 20200202 (2020).
[5] P. A. Butler, Phys. Scr. **99**, 035302 (2024).
[6] L. P. Gaffney, P. A. Butler, M. Scheck, A. B. Hayes, F. Wenander, M. Albers, B. Bastin, C. Bauer, A. Blazhev, S. Bönig, N. Bree, J. Cederkäll, T. Chupp, D. Cline, T. E. Cocolios, T. Davinson, H. D. Witte, J. Diriken, T. Grahn, A. Herzan, M. Huyse, D. G. Jenkins, D. T. Joss, N. Kesteloot, J. Konki, M. Kowalczyk, T. Kröll, E. Kwan, R. Lutter, K. Moschner, P. Napiorkowski, J. Pakarinen, M. Pfeiffer, D. Radeck, P. Reiter, K. Reynders, S. V. Rigby, L. M. Robledo, M. Rudigier, S. Sambi, M. Seidlitz, B. Siebeck, T. Stora, P. Thoele, P. V. Duppen, M. J. Vermeulen, M. von Schmid, D. Voulot, N. Warr, K. Wimmer, K. Wrzosek-Lipska, C. Y. Wu, and M. Zielinska, Nature (London) **497**, 199 (2013).
[7] B. Bucher, S. Zhu, C. Y. Wu, R. V. F. Janssens, D. Cline, A. B. Hayes, M. Albers, A. D. Ayangeakaa, P. A. Butler, C. M. Campbell, M. P. Carpenter, C. J. Chiara, J. A. Clark, H. L. Crawford, M. Cromaz, H. M. David, C. Dickerson, E. T. Gregor, J. Harker, C. R. Hoffman, B. P. Kay, F. G. Kondev, A. Korichi, T. Lauritsen, A. O. Macchiavelli, R. C. Pardo, A. Richard, M. A. Riley, G. Savard, M. Scheck, D. Seweryniak, M. K. Smith, R. Vondrasek, and A. Wiens, Phys. Rev. Lett. **116**, 112503 (2016).
[8] B. Bucher, S. Zhu, C. Y. Wu, R. V. F. Janssens, R. N. Bernard, L. M. Robledo, T. R. Rodríguez, D. Cline, A. B. Hayes, A. D. Ayangeakaa, M. Q. Buckner, C. M. Campbell, M. P. Carpenter, J. A. Clark, H. L. Crawford, H. M. David, C. Dickerson, J. Harker, C. R. Hoffman, B. P. Kay, F. G. Kondev, T. Lauritsen, A. O. Macchiavelli, R. C. Pardo, G. Savard, D. Seweryniak, and R. Vondrasek, Phys. Rev. Lett. **118**, 152504 (2017).
[9] K. Heyde, P. Van Isacker, M. Waroquier, J. L. Wood, and R. A. Meyer, Phys. Rep. **102**, 291 (1983).
[10] J. L. Wood, K. Heyde, W. Nazarewicz, M. Huyse, and P. van Duppen, Phys. Rep. **215**, 101 (1992).
[11] K. Heyde and J. L. Wood, Rev. Mod. Phys. **83**, 1467 (2011).
[12] P. E. Garrett, M. Zielińska, and E. Clément, Prog. Part. Nucl. Phys. **124**, 103931 (2022).
[13] S. Leoni, B. Fornal, A. Bracco, Y. Tsunoda, and T. Otsuka, Prog. Part. Nucl. Phys. **139**, 104119 (2024).
[14] R. F. Casten, Prog. Part. Nucl. Phys. **62**, 183 (2009).
[15] P. Cejnar, J. Jolie, and R. F. Casten, Rev. Mod. Phys. **82**, 2155 (2010).
[16] L. Carr, ed., *Understanding Quantum Phase Transitions* (CRC Press, 2010).
[17] L. Fortunato, Prog. Part. Nucl. Phys. **121**, 103891 (2021).
[18] D. Bès and R. Broglia, Nucl. Phys. **80**, 289 (1966).
[19] D. Bès, R. Broglia, and B. Nilsson, Phys. Lett. B **40**, 338 (1972).
[20] R. A. Broglia, O. Hansen, and C. Riedel, Two-neutron transfer reactions and the pairing model, in *Advances in Nuclear Physics: Volume 6*, edited by M. Baranger and E. Vogt (Springer US, Boston, MA, 1973) pp. 287–457.
[21] L. Próchniak, K. Zając, K. Pomorski, S. Rohoziński, and J. Srebrny, Nucl. Phys. A **648**, 181 (1999).
[22] D. M. Brink and R. A. Broglia, *Nuclear superfluidity: pairing in finite systems* (Cambridge University Press, 2005).
[23] J. Srebrny, T. Czosnyka, C. Droste, S. G. Rohoziński, L. Próchniak, K. Zając, K. Pomorski, D. Cline, C. Y. Wu, A. Bäcklin, L. Hasselgren, R. M. Diamond, D. Habs, H. J. Körner, F. S. Stephens, C. Baktash, and R. P. Kostecki, Nucl. Phys. A **766**, 25 (2006).
[24] L. Próchniak, Int. J. Mod. Phys. E **16**, 352 (2007).
[25] J. Xiang, Z. P. Li, T. Nikšić, D. Vretenar, and W. H. Long, Phys. Rev. C **101**, 064301 (2020).
[26] K. Nomura, D. Vretenar, Z. P. Li, and J. Xiang, Phys. Rev. C **102**, 054313 (2020).
[27] A. Bohr and B. R. Mottelson, *Nuclear Structure*, Vol. II (Benjamin, New York, USA, 1975).
[28] A. I. Levon, G. Graw, R. Hertenberger, S. Pascu, P. G. Thirolf, H.-F. Wirth, and P. Alexa, Phys. Rev. C **88**, 014310 (2013).

[29] M. Spieker, D. Bucurescu, J. Endres, T. Faestermann, R. Hertenberger, S. Pascu, S. Skalacki, S. Weber, H.-F. Wirth, N.-V. Zamfir, and A. Zilges, Phys. Rev. C **88**, 041303 (2013).
[30] M. Spieker, S. Pascu, D. Bucurescu, T. M. Shneidman, T. Faestermann, R. Hertenberger, H.-F. Wirth, N.-V. Zamfir, and A. Zilges, Phys. Rev. C **97**, 064319 (2018).
[31] N. V. Zamfir, J.-y. Zhang, and R. F. Casten, Phys. Rev. C **66**, 057303 (2002).
[32] D. A. Meyer, V. Wood, R. F. Casten, C. R. Fitzpatrick, G. Graw, D. Bucurescu, J. Jolie, P. v. Brentano, R. Hertenberger, H.-F. Wirth, N. Braun, T. Faestermann, S. Heinze, J. L. Jerke, R. Krücken, M. Mahgoub, O. Möller, D. Mücher, and C. Scholl, Phys. Rev. C **74**, 044309 (2006).
[33] S. Pascu, G. Căta-Danil, D. Bucurescu, N. Mărginean, N. V. Zamfir, G. Graw, A. Gollwitzer, D. Hofer, and B. D. Valnion, Phys. Rev. C **79**, 064323 (2009).
[34] S. Pascu, G. Căta-Danil, D. Bucurescu, N. Mărginean, C. Müller, N. V. Zamfir, G. Graw, A. Gollwitzer, D. Hofer, and B. D. Valnion, Phys. Rev. C **81**, 014304 (2010).
[35] D. Bucurescu, S. Pascu, G. Suliman, H.-F. Wirth, R. Hertenberger, T. Faestermann, R. Krücken, and G. Graw, Phys. Rev. C **100**, 044316 (2019).
[36] A. I. Levon, D. Bucurescu, C. Costache, T. Faestermann, R. Hertenberger, A. Ionescu, R. Lica, A. G. Magner, C. Mihai, R. Mihai, C. R. Nita, S. Pascu, K. P. Shevchenko, A. A. Shevchuk, A. Turturica, and H.-F. Wirth, Phys. Rev. C **102**, 014308 (2020).
[37] F. Iachello and A. Arima, *The interacting boson model* (Cambridge University Press, Cambridge, 1987).
[38] T. Otsuka, A. Arima, F. Iachello, and I. Talmi, Phys. Lett. B **76**, 139 (1978).
[39] T. Otsuka, A. Arima, and F. Iachello, Nucl. Phys. A **309**, 1 (1978).
[40] A. Arima and F. Iachello, Phys. Rev. C **16**, 2085 (1977).
[41] O. Scholten, F. Iachello, and A. Arima, Ann. Phys. (NY) **115**, 325 (1978).
[42] R. Fossion, C. E. Alonso, J. M. Arias, L. Fortunato, and A. Vitturi, Phys. Rev. C **76**, 014316 (2007).
[43] Y. Zhang and F. Iachello, Phys. Rev. C **95**, 034306 (2017).
[44] K. Nomura and Y. Zhang, Phys. Rev. C **99**, 024324 (2019).
[45] J. García-Ramos, J. Arias, and A. Vitturi, Chin. Phys. C **44**, 124101 (2020).
[46] P. Ring and P. Schuck, *The Nuclear Many-Body Problem* (Springer-Verlag, Berlin, 1980).
[47] M. Bender, P.-H. Heenen, and P.-G. Reinhard, Rev. Mod. Phys. **75**, 121 (2003).
[48] K. Nomura, N. Shimizu, and T. Otsuka, Phys. Rev. Lett. **101**, 142501 (2008).
[49] K. Nomura, N. Shimizu, and T. Otsuka, Phys. Rev. C **81**, 044307 (2010).
[50] K. Nomura, Eur. Phys. J. A **61**, 139 (2025).
[51] K. Nomura, R. Rodríguez-Guzmán, and L. M. Robledo, Phys. Rev. C **101**, 024311 (2020).
[52] K. Nomura, R. Rodríguez-Guzmán, and L. M. Robledo, Phys. Rev. C **101**, 044318 (2020).
[53] K. Nomura, Phys. Rev. C **109**, 034319 (2024).
[54] K. Nomura, Phys. Rev. C **105**, 044301 (2022).
[55] K. Nomura, Phys. Rev. C **112**, 054310 (2025).
[56] K. Nomura, Phys. Lett. B **871**, 139995 (2025).
[57] K. Nomura, Int. J. Mod. Phys. E **32**, 2340001 (2023).
[58] T. H. R. Skyrme, Nucl. Phys. **9**, 615 (1958).
[59] J. Bartel, P. Quentin, M. Brack, C. Guet, and H.-B. Håkansson, Nucl. Phys. A **386**, 79 (1982).
[60] K. Nomura, R. Rodríguez-Guzmán, and L. M. Robledo, Phys. Rev. C **92**, 014312 (2015).
[61] K. Nomura, R. Rodríguez-Guzmán, L. M. Robledo, J. E. García-Ramos, and N. C. Hernández, Phys. Rev. C **104**, 044324 (2021).
[62] L. M. Robledo, T. R. Rodríguez, and R. R. Rodríguez-Guzmán, J. Phys. G: Nucl. Part. Phys. **46**, 013001 (2019).
[63] J. Decharge, M. Girod, and D. Gogny, Phys. Lett. B **55**, 361 (1975).
[64] S. Goriely, S. Hilaire, M. Girod, and S. Péru, Phys. Rev. Lett. **102**, 242501 (2009).
[65] J. Engel and F. Iachello, Phys. Rev. Lett. **54**, 1126 (1985).
[66] J. Engel and F. Iachello, Nucl. Phys. A **472**, 61 (1987).
[67] J. N. Ginocchio and M. W. Kirson, Nucl. Phys. A **350**, 31 (1980).
[68] K. Nomura, Phys. Rev. C **106**, 024330 (2022).
[69] T. Otsuka, Phys. Lett. B **182**, 256 (1986).
[70] Brookhaven National Nuclear Data Center, `http://www.nndc.bnl.gov`.
[71] S. Pascu, E. Yüksel, Abhishek, P. Stevenson, G. H. Bhat, R. N. Mao, K. Nomura, C. Costache, Z. P. Li, N. Mărginean, C. Mihai, T. Naz, Z. Podolyák, P. H. Regan, A. E. Turturică, R. Borcea, M. Boromiza, D. Bucurescu, S. Călinescu, C. Clisu, A. Coman, I. Dinescu, S. Doshi, D. Filipescu, N. M. Florea, A. Gandhi, I. Gheorghe, A. Ionescu, R. Lică, R. Mărginean, R. E. Mihai, A. Mitu, N. Nazir, A. Negret, C. R. Niţă, E. B. O'Sullivan, C. Petrone, S. E. Poulton, J. A. Sheikh, H. K. Singh, L. Stan, S. Toma, G. Turturică, and S. Ujeniuc, Phys. Rev. Lett. **134**, 092501 (2025).
[72] D. G. Fleming, C. Günther, G. Hagemann, B. Herskind, and P. O. Tjøm, Phys. Rev. C **8**, 806 (1973).
[73] M. Shahabuddin, D. Burke, I. Nowikow, and J. Waddington, Nucl. Phys. A **340**, 109 (1980).
[74] G. Løvhøiden, T. Thorsteinsen, E. Andersen, M. Kiziltan, and D. Burke, Nucl. Phys. A **494**, 157 (1989).
[75] P. Debenham and N. M. Hintz, Nucl. Phys. A **195**, 385 (1972).
[76] J. Bjerregaard, O. Hansen, O. Nathan, and S. Hinds, Nucl. Phys. **86**, 145 (1966).
[77] V. Ponomarev, M. Pignanelli, N. Blasi, A. Bontempi, J. Bordewijk, R. De Leo, G. Graw, M. Harakeh, D. Hofer, M. Hofstee, S. Micheletti, R. Perrino, and S. van der Werf, Nucl. Phys. A **601**, 1 (1996).
[78] P. E. Garrett, W. D. Kulp, J. L. Wood, D. Bandyopadhyay, S. Choudry, D. Dashdorj, S. R. Lesher, M. T. McEllistrem, M. Mynk, J. N. Orce, and S. W. Yates, Phys. Rev. Lett. **103**, 062501 (2009).
[79] Y. Tsunoda, N. Shimizu, and T. Otsuka, Phys. Rev. C **108**, L021302 (2023).
[80] K. Nomura, D. Vretenar, T. Nikšić, and B.-N. Lu, Phys. Rev. C **89**, 024312 (2014).
[81] K. Nomura, R. Rodríguez-Guzmán, Y. M. Humadi, L. M. Robledo, and J. E. García-Ramos, Phys. Rev. C **102**, 064326 (2020).
[82] D. D. Warner and R. F. Casten, Phys. Rev. C **28**, 1798 (1983).

[83] R. Chapman, W. McLatchie, and J. Kitching, Nucl. Phys. A **186**, 603 (1972).